Available online at www.sciencedirect.com

ScienceDirect

Physics Procedia 88 (2017) 266 – 274

Physics Procedia

8th International Topical Meeting on Neutron Radiography, Beijing, China, 4-8 September 2016

Which resolution can be achieved in practice in neutron imaging experiments? – A general view and application on the Zr - ZrH_2 and ZrO_2 - ZrN systems

Mirco Grosse[a,*], Nikolay Kardjilov[b]

[a] *Karlsruhe Institute of Technology, Hermann-von-Helmholtz-Platz 1, Eggenstein-Leopoldshafen 76344, Germany*
[b] *Helmholtz Center Berlin, Germany*

Abstract

Current methodical developments improve the spatial resolution of neutron imaging facilities. Objects with dimensions down to several microns should be detectable. However, the minimum object size detectable depends not only on the facility hardware like detector resolution or neutron optics, but also on the attenuation contrast. In this paper the relation between illumination time needed, neutron contrast of the objects and their minimal size detectable is derived and an analysis of the minimal dimension of an object can be detected in neutron radiography and tomography is discussed at two examples: zirconium hydride ZrH_2 in Zircaloy-4 as a high contrast system and zirconium nitride ZrN in zirconium oxide ZrO_2 as a low contrast system. It is concluded which minimal sizes of the precipitates can be detected in realistic times.

Peer-review under responsibility of the organizing committee of ITMNR-8

Keywords: neutron imaging, resolution, Zircaloy-4, zirconium hydride, zirconium nitride, zirconium oxide

1. Introduction

Precipitates with dimensions in the order of magnitude of 1 to 10 µm play important roles for material properties. Zirconium alloys are applied e.g. for nuclear fuel claddings or pressure tubes. Under operation, accidents or long term storage conditions their mechanical and chemical properties are strongly influenced by two characteristic

* Corresponding author. Tel.: +49 721 608 23884; fax: +49 721 608 24567.
E-mail address: Mirco.Grosse@KIT.edu

Peer-review under responsibility of the organizing committee of ITMNR-8
doi:10.1016/j.phpro.2017.06.037

micro-structural features: The formation of nitrides in the oxide layer on zirconium alloy strongly accelerates the further oxidation kinetics. The nitrides can be formed if zirconium reacts in air or steam-nitrogen atmospheres. It can happen in spent fuel accidents or in the late phase of a severe reactor accident after failure of the pressure vessel. Fig. 1 gives an example of a typical ZrO_2/ZrN microstructure near the metal-oxide interface. The sizes of these nitrides are several micrometers. Another example is zirconium hydride in zirconium alloys (see Fig. 2). Hydrogen is absorbed by zirconium alloys as result of corrosion under operation conditions or by the reaction with steam at high temperatures under accident conditions. Typical dimensions of these rod shaped precipitates are 1 - 2 µm thickness and 10 - 20 µm length. They are decreasing the fracture toughness of the metal and provide the risk of the so called delayed hydride cracking and/or the fragmentation of the fuel rods during emergency cooling of an overheated reactor, both resulting in fission gas release and redistribution of fuel. Usual these hydrides are oriented in circumferential direction. Under certain stress conditions the can be re-oriented in radial direction. In this case they degrade the mechanical properties much stronger.

Neutron imaging is used by several groups to study the hydrogen in zirconium (for instance Yasuda et al. 2002, Lehmann et al. 2003, Grosse et al. 2008, Grosse et al. 2011, Wang et al. 2013, Smith et al. 2015, Tremsin et al, 2015) . Currently, nominal spatial resolutions of typical 25 to 80 µm were used for these investigations (pixel sizes between 13.6 and 40 µm). Integral information about the hydrogen content averaged over the corresponding gauge volume was obtained. Fig. 3 shows as an example the 3D reconstruction of the hydrogen distribution measured in a zirconium ally cladding tube exposed to a loss of coolant simulation test.. It can clearly be seen that the cladding tube brokes at a hydrogen enrichment. However, for deeper understanding of the precipitation, re-solution and re-orientation processes, knowledge about formation, amount, re-distribution and re-orientation of the individual precipitates in the bulk of the materials at the temperatures at which it occurs would be very helpful. In-situ neutron imaging with high spatial resolution could provide this information because of the penetration depth of neutrons in matter allowing dedicated sample environments.

However, currently the spatial resolutions of these methods which are in the order of 20 µm are not yet sufficient. Actually, a lot of efforts are made at several neutron imaging beamlines to improve the spatial resolution of the method (e.g. Tremsin et al. 2011, Hussey et al. 2015, Trtik et al. 2015, Bingham et al. 2015, Trtik et al. 2016a). Spatial resolution down to 1 µm seems to be reachable. The application of neutron optics together with high resolution detector systems seems to allow reducing the spatial resolution even below the 1 µm limit.

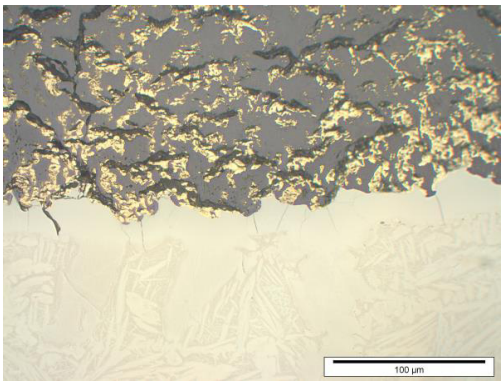

Fig. 1. Optical microstructure of the oxide layer on Zry-4 after 40 min reaction in 20 % steam + 80 % N_2 atmosphere at 1100°C (yellow: ZrN, bright gray: Zry-4, dark gray: ZrO_2, black: micro-cracks).

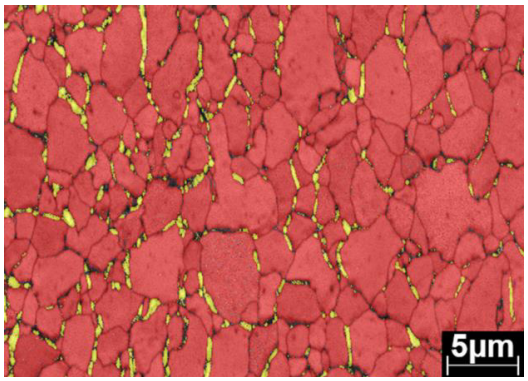

Fig. 2. EBSD pattern of a hydrided Zircaloy-4 sample (yellow: Zirconium hydrides (yellow), red: Zircaloy-4 (Pshenichnikov et al. 2016)

On the other hand, resolution in the neutron imaging experiment is a multidimensional parameter (two or three lateral dimensions for radiography or tomography, respectively, resolution of contrast, time and neutron wavelength) as mentioned in (Griesche et al. 2016). These parameters cannot be varied independently. A decrease of the minimal size detectable by neutron imaging is penalized by an increase in the illumination time per radiograph and/or a

decrease in the neutron wavelength resolution. The illumination time as well the wavelength range used cannot be varied unlimited. The limit for the wavelength range is the whole neutron spectrum, the limits for the illumination time is 1-5 days corresponding to the beam time usually obtained as an external user.

Therefore, about the question of the immanent limitations for the resolution of neutron imaging arises. This question is discussed in this paper using as a simple model a single cube-shaped object in a sample with homogeneous matrix. For the analysis two examples are used: zirconium hydride, ZrH_2, in Zircaloy-4 (Zry-4) as a high contrast system and zirconium nitride, ZrN, in zirconium oxide ZrO_2 as a low contrast system. The neutron source parameters valid for the CONRAD facility at the Berlin Neutron Scattering Centre BENSC (Germany) are used as basis for the estimations.

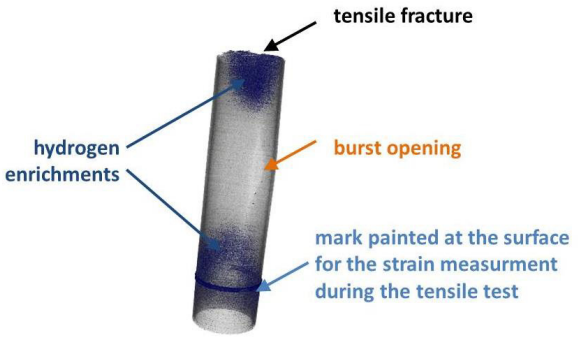

Fig.3. Reconstruction of the hydrogen distribution in an zirconium alloy cladding tube close to burst opening reconstructed from neutron tomography data measured at CONRAD (BENSC Berlin, Germany).

2. Dependence of the illumination time needed on the precipitation size

In the following the discussion is focused on the classical neutron radiography using a pinhole camera setup where the contrast is caused only at differences in the total macroscopic neutron cross sections:

$$\Sigma = N\left(\sigma_c + \sigma_i + \sigma_a\right) \tag{1}$$

Σ is the total macroscopic neutron cross section, σ_c, σ_i and σ_a the microscopic coherent, incoherent and absorption neutron cross section, respectively. Not discussed are effects in special systems which can result in additional contrasts like phase shifts, Frauenhofer diffraction, total reflection or refraction at interfaces.

Furthermore, the efficiencies of camera and transmitter foil are not included in the discussion. For the transmitter foil it has to be taken into account that an amplification of the photons to neutron ratio, as obtained by using LiF, does not increase the contrast resolution.

2.1. Neutron Radiography

The basis of the contrast in a neutron radiograph is the Lambert- Beer law:

$$\frac{I(x,y)}{I_0(x,y)} = T(x,y) = \exp\left(-\sum_i \Sigma_i(x,y)\, s_i(x,y)\right) \tag{2}$$

$I(x,y)$ and $I_0(x,y)$ are the intensities counted at pixel x,y with and without sample, respectively, $T(x,y)$ is the transmission and s_i the neutron path length through the phase i. Fig. 4 gives the dependence of the neutron transmission on the precipitate size calculated with the cross sections given in Tab. 1 (The cross sections depend on the neutron spectrum used by the facility. The values are valid for ICON (PSI Villigen, ANTARES (MLZ Garching

and CONRAD (BENSC Berlin) having similar cold neutron spectra (Grieche et al. 2016). The total hydrogen neutron cross section of BOA (PSI Villigen) is higher whereas for NEUTRA (PSI Villigen) using thermal neutrons is lower).

$I_0(x,y)$ can be replaced by

$$I_0(x,y) = \frac{\phi_0}{\left(L/d\right)^2} s_{pixel}^2 \, t \tag{3}$$

ϕ_0 is a virtual neutron flux estimated for $L/d = 1$, L the distance between aperture and detector, d the opening of the aperture slit, s_{pixel} the pixel size and t the time. To detect a small object by means of neutron imaging it is not only necessary that the detector resolution is smaller than the size of the object s_0

$$s_{pixel} < s_O \tag{4}$$

The object has to give a contrast beyond the intensity noise caused by the counting statistic and the background intensity I_B

$$\Delta I > \frac{\sqrt{I + I_B}}{I - I_B} \tag{5}$$

Tab. 1 Total macroscopic neutron cross sections used for the analysis

Phase	Σ_{total}, cm^{-1}	reference
Zry-4	0.21	Grosse et al. 2008
ZrH_2	5.80	
ZrN	0.814	Sears 1992
ZrO_2	0.443	

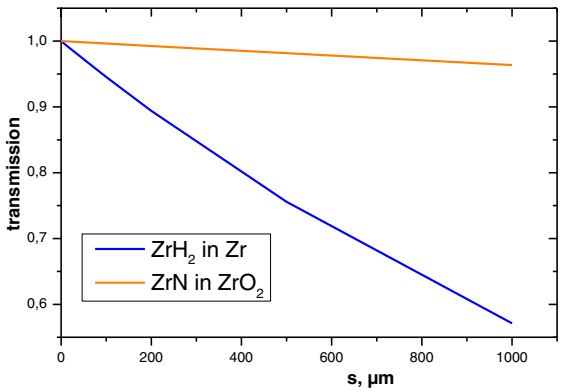

Fig. 4. Dependence of neutron transmission on the precipitate size.

For very small objects $I_O \approx I_M$ is valid (I_O is the pixel intensity at object position and I_M the pixel intensity of the matrix without object). From Eqs. (2) and (5) it can be derived

$$\frac{|I_O - I_M|}{I_M} = |T_O - 1| = \left|1 - \exp\left(-(\Sigma_O - \Sigma_M)\, s_O\right)\right| > \frac{\sqrt{I_M + I_B}}{I_M - I_B} \tag{6}$$

Neglecting the background intensity if $I_B << I_M$, the intensity needed to detect an object of size s_O is given by

$$I_M(x,y) = \frac{\phi_1}{\left(L/d\right)^2} \exp\left(-\Sigma_M\ s_M\right) s_{pixel}^2\ t > \left(\frac{1}{1-\exp\left(-\left(\Sigma_O - \Sigma_M\right) s_O\right)}\right)^2 \tag{7}$$

Fig. 5 plots the dependence of the counts needed to detect a single zirconium hydride in Zircaloy-4 and zirconium nitride in zirconium oxide, respectively, on the size of the precipitates. The beam divergence is sufficient to detect a small object if the condition

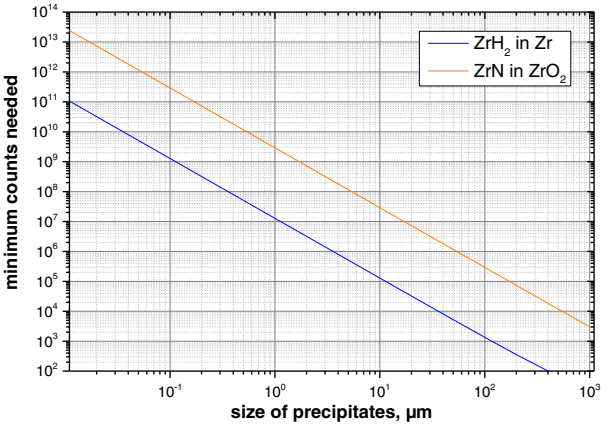

Fig. 5. Dependence of the counts needed to detect a precipitate on the precipitate size for ZrH_2 in Zry-4 and ZrN in ZrO_2, respectively.

$$L/d \geq l/s_O \tag{8}$$

is fulfilled with l as the distance between sample and neutron transmitter. A simplified relation between illumination time and pixel resolution can be derived from Eqs. (7) and (8) under the conditions that the pixel size should be half of the object size $s_{pixel} = s_O/2$, the intensity contrast should be double of intensity scattering due to the counting statistics $\Delta I = 2\sqrt{I}$, and small samples are applied with $\exp\left(-\Sigma_M\ s_M\right) \approx 1$:

$$\frac{\phi_1\ s_O^4}{2\,l^2}\,t = 2\left(\frac{1}{1-\exp\left(-\left(\Sigma_O - \Sigma_M\right) s_O\right)}\right)^2 \tag{9}$$

From this equation the illumination time needed to detect a single precipitate can be calculated by

$$t = \frac{4\,l^2}{\phi_1\ s_O^4\left(1-\exp\left(-\left(\Sigma_O - \Sigma_M\right) s_O\right)\right)^2} \tag{10a}$$

As examples, the illumination time needed to detect a single ZrH_2 precipitate in Zry-4 and a single ZrN precipitate in ZrO_2 calculated for the CONRAD beamline at BENSC on the basis of a distance between sample and transmitter of 1 mm is plotted in Fig. 6. From these calculations it can be concluded that the limit to detect a single particle at this beamline is about 40 µm for ZrH_2 in Zry-4 and about 150 µm for ZrN in ZrO_2.

The general relation between spatial, time, contrast and wavelength resolution can be described by Eq. (9) too:

$$\Delta t = \frac{4\,l^2}{\phi_1(\Delta\lambda,\lambda)\ s_O^4\left(1-\exp\left(-\Delta\Sigma\ s_O\right)\right)^2} \tag{10b}$$

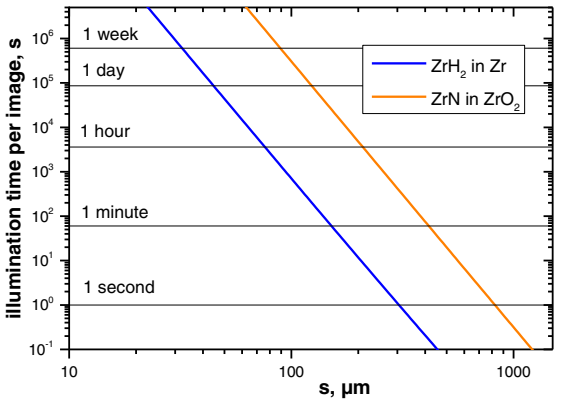

Fig. 6. Dependence of illumination time needed at CONRAD on the size of the object.

2.2. Neutron Tomography

The sampling theorem for tomography investigations gives the number of projections needed for a reconstruction without losing information.

$$N_{projections} = \frac{\pi}{2}\frac{R_{sample}}{s_{pixel}} \tag{11a}$$

with the number of projection needed $N_{projections}$ and R_{sample} as the ratio of the circle including the whole sample. The two parameters can be substituted as following: R_{sample} can be replaced by the half of the sample width $s_M/2$ and s_{pixel} by $s_O/2$ according the discussion above:

$$N_{projections} = \frac{\pi}{2}\frac{2\,s_M}{2\,s_O} = \frac{\pi}{2}\frac{s_M}{s_O} \tag{11b}$$

It follows that the time needed for a tomography neglecting the time for positioning and readout is given by

$$t = \frac{\pi}{2}\frac{s_M}{s_O}\frac{4\,l^2}{\phi_1\,s_O^4\left(1-\exp\left(-\left(\Sigma_O-\Sigma_M\right)s_O\right)\right)^2} = \frac{2\,\pi\,s_M\,l^2}{\phi_1\,s_O^5\left(1-\exp\left(-\left(\Sigma_O-\Sigma_M\right)s_O\right)\right)^2} \tag{12}$$

Fig. 7 gives the size dependence of the time needed for a tomography for the two systems discussed.

Fulfilling the sampling theorem provides in principle the upper bound (the worst case scenario) for the time required for tomography. In this regard different noise reducing filter techniques like sinogram inpainting (Arcadu et al 2001), can be applied in order to reduce the time needed for tomography significantly. For future experimental confirmation of the determined resolution limits here the obtained images/datasets can be evaluated using Fourier ring/shell correlation technique. This technique is routinely used for assessment of spatial resolution of the images/3D datasets for number of various microscopic techniques (Mizutani et al.2016).

3. Discussion

This analysis is valid for facilities using pinhole geometry and for cubic or cube-like objects. Often rod- or disc-shaped objects extended in one or two dimensions, respectively, are of interest. Examples are for instance joining's between components or plane cracks. For cracks additional contrast can occur caused by refraction or total reflection

if the crack is oriented suitably. For such objects the dimension in neutron path direction determines the contrast between object and matrix.

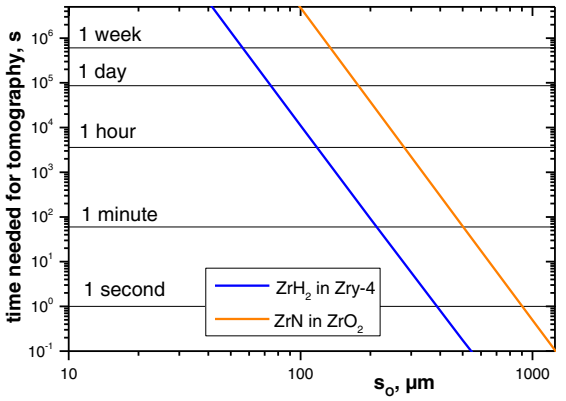

Fig. 7. Dependence of time needed for a tomography at CONRAD on the size of the object.

The application of neutron lenses can increase the intensity available by a factor up to 100 (Hussey et al. 2015) because no or at least less requirements of beam collimation is needed compared to the classical pinhole camera. The consequence is a reduction of the exponent of the object size s_O in the correlation with illumination times needed given by Eq.(10a and b) by a factor of 2. However, even in setups using neutron lenses general estimations of the minimal object size have to be performed.

On the first glance the results presented in this analysis seem contradicting former own experiments with a nominal spatial resolution of about 25 µm. However, in these former neutron radiography measurements no single hydrides but the hydrogen concentration averaged over the whole neutron path length through the material (1.45 … 5.4 mm depending on the sample position) was investigated. Thousands of zirconium hydride precipitates along the neutron path give the contrast needed to see it in the image.

The situation is different for neutron tomography investigations with voxel volumes of minimal 13.6 µm * 13.6 µm * 13.6 µm. In these tomography measurements the condition that values of hydride containing voxels should completely distinguished from voxel values without hydrides was not fulfilled. The scattering bands of both types overlapped. The human mind is able to recognize and divide sample pattern even if their scattering bands overlap by interpolation and closing of areas. Therefore, positions of hydride enrichments could be detected by these measurements at least in a scale of hundreds of microns. The problem of overlapping scattering bands become obviously when a computer based statistical data analysis was performed to quantify mean and maximal hydrogen concentrations depending on the axial cladding tube position (Muttini 2015). Here at first the voxels being in the sample has to be divided from voxels outside the sample. This was done by defining regions of interest using binary images. It was not possible to find threshold voxel values distinguishing sample inside and outside. Some voxels outside the sample has too high and some voxels inside the sample too low values. In order to determine the sample positions several binary operations like spot cleaning, multiple dilatation and erosion and median calculations has to be applied. However, these operations decrease the spatial resolution and objects with a size smaller than nine voxels could no longer be detected. Therefore, the nominal spatial resolution of 25 µm applied was a “blind” resolution, meaning that the real resolution achieved was not as good as the nominal resolution looks like. In later neutron tomography investigations of the hydrogen distribution in nuclear fuel cladding tubes a more realistic spatial resolution of 40 .. 80 µm was applied.

4. Conclusions

Resolution in neutron imaging is a multidimensional ellipsoid surface at which the different components can be varied. For pinhole camera setups the different dimensions of resolution are connected as following:

The time resolution Δt is proportional to

- the spatial resolution for radiography by $s_O^{-4}\,(1-\exp(-\Delta\Sigma\, s_O))^{-2}$
  and for tomography by $s_O^{-5}\,(1-\exp(-\Delta\Sigma\, s_O))^{-2}$
- the wavelength resolution by $\phi_1(\Delta\lambda,\lambda)^{-1}$
- the contrast in the total macroscopic neutron cross section by $(1-\exp(-\Delta\Sigma\, s_O))^{-2}$

For the discussed systems ZrH_2 in Zry-4 and ZrN in ZrO_2 the minimal object dimensions detectable by means of neutron radiography are about 40 µm and about 100 µm, respectively if a neutron source of the power of the BER reactor is applied. For neutron tomography the minimal dimensions are about 60 µm and about 150 µm, respectively, under these conditions. For systems with larger difference in the total macroscopic neutron cross sections like MgB_2 fibers in a nickel matrix (Trtik 2016b) or even black absorbers much smaller objects can be detected.

It has to be concluded that the behavior whether of a single zirconium nitrides in zirconium oxide neither of single zirconium hydrides in Zircaloy-4 can be studied yet by means of neutron imaging. For the higher resolutions needed for these investigations much stronger neutron sources with orders of magnitude higher neutron fluxes are needed.

Acknowledgements

The authors thank all colleagues for the fruitful discussions. The investigations of the systems Zr - H and Zr - O - N - H with spatial resolution of about 0.1 mm were performed at ICON and BOA at SINQ, PSI Villigen, Switzerland, ANTARES at FRM2, TU Munich, Germany and CONRAD at BER, Helmholtz Center Berlin, Germany. Many thanks for providing beam time.

References

Arcadu, F., Vogel, J., Stampanoni, M., Marone, F., 2001. Improving analytical tomographic reconstructions through consistency conditions, Fundamenta Informaticae XXI 1001 - 1016

Bingham, P., Santos-Villalobos, H., Lavrik, N., Gregor, J., Bilheux, H., 2015. Magnified neutron radiography with cold sources, Physics Procedia, 69, 218 – 226

Griesche, A., Grosse, M., Schillinger, B., 2016. Neutron imaging, in Fritzsche, H., Huot, Fruchart, D.. (Eds), Neutron Scattering and Other Techniques for Hydrogen in Metals.

Grosse, M. , Kuehne, G., Steinbrueck, M., Lehmann, E., Stuckert, J., Vontobel, P., 2008, Quantification of hydrogen uptake of steam-oxidized zirconium alloys by means of neutron radiography, J. Phys. Cond. Matter 20, 104263

Grosse, M., van den Berg, N., Goulet, C., Lehmann, E., Schillinger B., 2011, In-situ neutron radiography investigations of hydrogen diffusion and absorption in zirconium alloys, Nucl. Instr.& Meth. In Phys. Res. A 651, 253 – 257

Hussey, D. S., Brocker, C., Cook, J. C., Jacobson, D. L., Gentile, T. R., Chen, W. C., Baltic, E., Baxter, D. V., Foskow, J., Arif, M., 2015. A New Cold Neutron Imaging Instrument at NIST, Physics Procedia, 69, 48 – 54

Lehmann, E., Vontobel, P. and Hermann, A., 2003, Non-destructive analysis of nuclear fuel by means of thermal and cold neutrons, Nucl. Instr. Meth., Vol. A 515, 745 – 759

Mizutani, R., Saiga, R., Takekoshi, S., Inomoto, C., Nakamura, N., Itokawa, M., Arai, M., Oshima, K., Takeuchi, A., Uesuhi, K., Terada, Y., Suzuki, Y., 2016. A method for estimating spatial resolution of real image in the Fourier domain, Journal of Microscopy, 261, 57 – 66

Muttini, E., 2015. Analysis and quantification of the hydrogen uptake of cladding tubes made of zirconium alloys during loss of coolant accidents (LOCA), master thesis, KIT and Université Paris-Sud

Pshenichnikov, A., Stuckert, J., Walter, M., 2016. Hydride precipitation, fracture and plasticity mechanisms in pure zirconium and Zircaloy-4 at temperatures typical for the postulated loss-of-coolant accident, Nucl. Engin. & Design 301, 366 – 377

Sears V. F., 1992. Neutron scattering lengths and cross sections, Neutron News 3, 26 – 37

Smith, T., Bilheux, H., Ray, H., Bilheux, J. C. and Yan Y., 2015, Nonondestructive Evaluation of Hydrided Zircaloy-4 Cladding Materials by Neutron Radiography and Tomography, Phys. Proc., 69, 478 - 482

Tremsin, A. S., McPhate, J. B., Vallerga, J. V. Siegmund, O. H. W., Feller, W. B., Lehmann, E., Dawson, M, 2011. Improved efficiency of high resolution and cold neutron imaging, Nucl. Instr. & Meth in Phys. Res. A 628, 415 – 418

Tremsin, A.S., Morgano, M. Panzner, T., Lehmann, E. Filgers, U., Vallerga, J.V., McPhate, J.B., Siegmund, O.H.W. Feller, W.B., 2015, High resolution neutron imaging capabilities at BOA beamline at Paul Scherrer Institut, Nucl. Instrm. & Meth., Vol. A784, 486 - 493

Trtik, P., Hovind, J., Grünzweig, C., Bollhalder, A., Thominet, V., David, C., Kaestner, A., Lehmann, E. H., 2015. Improving the spatial resolution of neutron imaging at Paul Scherrer Institut – The Neutron Microscope Project, Physics Procedia, 69, 169 – 176

Trtik, P., Lehmann E. H., 2016a, Progress in High-resolution Neutron Imaging at the Paul Scherrer Institut – The Neutron Microscope Project, Journal of Physics: Conference Series 746, 012004

Trtik, P., 2016b, High-resolution neutron tomography of superconducting multifilament MgB2 wires, ITMNR-8 Bejing, September 4 – 8 2016

Wang, Z., Garbe, U., Li, H., Harrison, R. P., Toppler, K., Studer, A. J., Palmer, T., Planchenault, G., 2013. Hydride precipitation and ist influence on mechanical properties of notched and unnotched Zircaloy-4 plates, J. Nucl. Mater. 436, 84 – 92

Yasuda, R., Matsubayashi, M., Nakata, M. and Harada, K., 2002, Application of neutron radiography for estimating concentration and distribution of hydrogen in Zircaloy cladding tubes, J. Nucl. Mater., Vol. 302, 156 - 164.